





Brief Report

SARS-CoV-2 Variants of Concern Infect the Respiratory Tract and Induce Inflammatory Response in Wild-Type Laboratory Mice

Shannon Stone [†], Hussin Alwan Rothan [†] , Janhavi Prasad Natekar , Pratima Kumari, Shaligram Sharma , Heather Pathak, Komal Arora, Tabassum Tasnim Aurooni and Mukesh Kumar ^{*} 

Department of Biology, College of Arts and Sciences, Georgia State University, Atlanta, GA 30303, USA; sstone12@student.gsu.edu (S.S.); hrothan@gsu.edu (H.A.R.); jnatekar1@gsu.edu (J.P.N.); pkumari1@gsu.edu (P.K.); ssharma17@student.gsu.edu (S.S.); hpathak1@gsu.edu (H.P.); karora@gsu.edu (K.A.); tauroni1@student.gsu.edu (T.T.A.)

^{*} Correspondence: mkumar8@gsu.edu

[†] These authors contributed equally to this work.

Abstract: The emergence of new severe acute respiratory syndrome coronavirus-2 (SARS-CoV-2) variants of concern pose a major threat to public health, due to possible enhanced virulence, transmissibility and immune escape. These variants may also adapt to new hosts, in part through mutations in the spike protein. In this study, we evaluated the infectivity and pathogenicity of SARS-CoV-2 variants of concern in wild-type C57BL/6 mice. Six-week-old mice were inoculated intranasally with a representative virus from the original B.1 lineage, or the emerging B.1.1.7 and B.1.351 lineages. We also infected a group of mice with a mouse-adapted SARS-CoV-2 (MA10). Viral load and mRNA levels of multiple cytokines and chemokines were analyzed in the lung tissues on day 3 after infection. Our data show that unlike the B.1 virus, the B.1.1.7 and B.1.351 viruses are capable of infecting C57BL/6 mice and replicating at high concentrations in the lungs. The B.1.351 virus replicated to higher titers in the lungs compared with the B.1.1.7 and MA10 viruses. The levels of cytokines (IL-6, TNF- α , IL-1 β) and chemokine (CCL2) were upregulated in response to the B.1.1.7 and B.1.351 infection in the lungs. In addition, robust expression of viral nucleocapsid protein and histopathological changes were detected in the lungs of B.1.351-infected mice. Overall, these data indicate a greater potential for infectivity and adaptation to new hosts by emerging SARS-CoV-2 variants.

Keywords: COVID-19; SARS-CoV-2 variants; C57BL/6 mice; host-range; inflammation



Citation: Stone, S.; Rothan, H.A.; Natekar, J.P.; Kumari, P.; Sharma, S.; Pathak, H.; Arora, K.; Aurooni, T.T.; Kumar, M. SARS-CoV-2 Variants of Concern Infect the Respiratory Tract and Induce Inflammatory Response in Wild-Type Laboratory Mice. *Viruses* **2022**, *14*, 27. <https://doi.org/10.3390/v14010027>

Academic Editor: F. Javier Salguero

Received: 19 November 2021

Accepted: 22 December 2021

Published: 24 December 2021

Publisher's Note: MDPI stays neutral with regard to jurisdictional claims in published maps and institutional affiliations.



Copyright: © 2021 by the authors. Licensee MDPI, Basel, Switzerland. This article is an open access article distributed under the terms and conditions of the Creative Commons Attribution (CC BY) license (<https://creativecommons.org/licenses/by/4.0/>).

1. Introduction

Coronaviruses are a family of positive-sense single-strand RNA viruses. Their large genomes and propensity for mutation have resulted in a diversity of coronavirus strains that are capable of adapting to new hosts. COVID-19, the disease caused by the new beta coronavirus, SARS-CoV-2, has caused significant human and economic burden [1–3]. As of 10 December 2021, the number of confirmed cases worldwide is over 269 million, with 5.29 million deaths. Few therapies are available to treat COVID-19 in humans, and the rapid evolution of SARS-CoV-2 variants threatens to diminish their efficacy [2,4]. The lineage B.1.1.7, first identified in the United Kingdom, and lineage B.1.351, first described in South Africa, have been termed variants of concern because of the greater risk they pose due to their possible enhanced transmissibility, disease severity and immune escape [4–7]. These variants may also adapt to new hosts, in part, through mutations on the receptor-binding domain (RBD) of the spike protein [6,7].

SARS-CoV-2 infection begins with the viral particles binding to the receptors on the host cell surface. The RBD of the spike protein binds to angiotensin-converting enzyme 2 (ACE-2), present on the host cellular surfaces [3,8]. The RBD of the spike protein from the SARS-CoV-2 strain (Wuhan strain, lineage B.1) that started the pandemic does not

efficiently bind mouse ACE-2, and therefore wild-type laboratory mice are not susceptible to infection with lineage B.1 virus [8–12]. A mouse-adapted SARS-CoV-2 variant (MA10) with binding affinity to mouse ACE-2 has been obtained, after the sequential passaging of the virus in mouse lung tissue [11]. Infection of wild-type BALB/c mice with the MA10 virus resulted in replication in both the upper and lower airways [11,13]. The MA10 virus has several mutations, including multiple mutations in the spike protein compared with the Wuhan reference sequence. These mutations are also present in the B.1.1.7 lineage that first emerged in the UK, and the B.1.351 lineage that emerged independently of B.1.1.7 in South Africa. The B.1.1.7 variant has a mutation in the RBD of the spike protein, including N501Y, 69/70 deletion and P681H near the S1/S2 furin cleavage site. The B.1.351 variant has eight mutations, most notable are the three mutations (K417N, E484K and N501Y) in the RBD of spike protein [6,7,11,14,15]. This is associated with critical public health importance, since these mutations have been implicated in an increased recognition of mouse ACE2, hinting that the naturally emerging SARS-CoV-2 variants, including B.1.1.7 and B.1.351 may have evolved to infect rodents. However, the infectivity and pathogenicity of these emerging variants in mice have not yet been determined.

In this study, we evaluated the replication and pathogenicity of the original B.1 lineage and emerging SARS-CoV-2 lineages, B.1.1.7 and B.1.351, in wild-type C57BL/6 mice. We also used a mouse-adapted SARS-CoV-2 variant (MA10) that causes disease in the wild-type mice [11]. Our data show that the B.1.1.7 and B.1.351 viruses are capable of infecting wild-type C57BL/6 mice and replicating at high concentrations in the lungs. The B.1.351 virus replicated to higher titers in the lungs compared with the B.1.1.7 and MA10 viruses. We found that infection with the B.1.351, B.1.1.7 and MA10 viruses trigger an inflammatory response in the lungs characterized by upregulation of inflammatory cytokines and chemokines, and infiltration of leukocytes.

2. Materials and Methods

2.1. Animal Infection Experiments

C57BL/6 mice were purchased from the Jackson Laboratory (Bar Harbor, ME). All the animal experiments were conducted in a certified Animal Biosafety Level 3 (ABSL-3) laboratory at Georgia State University (GSU). The protocol was approved by the GSU Institutional Animal Care and Use Committee (Protocol number A20044). Six-week-old C57BL/6 mice were inoculated intranasally with PBS (mock) or 10^5 plaque-forming units (PFU) of SARS-CoV-2 as described previously [16]. We used B.1 Wuhan virus (BEI# NR-52281), B.1.1.7 virus (BEI# NR-54000), B.1.351 virus (BEI# NR-54008) and MA10 virus (BEI# NR-55329). Roughly equal numbers of male and female mice were used. Animals were weighed and their appetite, activity, breathing and neurological signs were assessed twice daily. In independent experiments, mice were inoculated with PBS (Mock) or SARS-CoV-2 intranasally, and on day 3 after infection, animals were anesthetized using isoflurane and perfused with cold PBS. The lungs were collected and flash-frozen in 2-methylbutane (Sigma, St. Louis, MO, USA) for further analysis, as described below [16,17]. Alternatively, mice were perfused with PBS, followed by 4% paraformaldehyde (PFA), and tissues were harvested, cryoprotected in 30% sucrose (Sigma, St. Louis, MO, USA), and embedded in optimum cutting temperature (OCT), as described previously [16,17].

2.2. Quantification of the Virus Load

The virus titers were analyzed in the lungs by plaque assay and quantitative real-time PCR (qRT-PCR). Briefly, frozen tissues were weighed and homogenized in a bullet blender (Next Advance, Averill Park, NY, USA) using stainless steel beads. Virus titers in tissue homogenates were measured by plaque assay using Vero cells [16,17]. Quantitative RT-PCR was used to measure viral RNA levels with primers and probes specific for the SARS-CoV-2 N gene as described previously [18]. Viral genome copies were determined by comparison to a standard curve generated using a known amount of RNA extracted from previously titrated SARS-CoV-2 samples [18]. Frozen tissues harvested from mock and

infected animals were weighed and lysed in RLT buffer (Qiagen), and RNA was extracted using a Qiagen RNeasy Mini kit (Qiagen, Germantown, MD, USA) [17,19]. Total RNA extracted from the tissues was quantified and normalized, and viral RNA levels per μg of total RNA were calculated.

2.3. Analysis of Cytokines and Chemokines

Total RNA was extracted from the lungs using a Qiagen RNeasy Mini kit (Qiagen, Germantown, MD, USA). cDNA samples were prepared using an iScript™ cDNA Synthesis Kit (Bio-Rad). The expression levels of multiple host genes were determined using qRT-PCR, and the fold change in infected lungs compared to the mock-infected controls was calculated after normalizing each sample to the level of the endogenous GAPDH gene mRNA [16,17,19]. The primer sequences used for qRT-PCR are listed in Table 1.

Table 1. Primer sequences used for qRT-PCR.

Gene (Accession No.)	Primer Sequence (5'–3')
IL-1 β (NM_000576)	Forward
	Reverse
IL-6 (NM_000600)	Forward
	Reverse
TNF- α (NM_013693)	Forward
	Reverse
CCL2 (NM_011333)	Forward
	Reverse

2.4. Histopathological Analysis

Lung sections were stained with hematoxylin and eosin (HE) for histopathological evaluation [16,17]. Additionally, tissue sections were incubated with anti-SARS-CoV-2 nucleocapsid antibody (Thermo Fisher Scientific, Norcross, GA, USA) overnight at 4 °C, followed by incubation with Alexa Fluor 555-conjugated secondary antibody (Invitrogen) for 1 h at room temperature. Images were acquired using the Invitrogen™ EVOS™ M5000 Cell Imaging System (Thermo Fisher Scientific, Norcross, GA, USA).

2.5. Immunoblot Analysis

Total cellular protein was extracted from mouse lungs and separated by SDS-PAGE, transferred onto PVDF membranes and incubated overnight with polyclonal antibody against IL-6 (Thermo Fisher Scientific, Norcross, GA, USA) [16,17]. Membranes were stripped and re-probed with antibodies against GAPDH (Proteintech). Following incubation with the secondary antibodies conjugated with IRDye 800 and IRDye 680 (Li-Cor Biosciences, Lincoln, NE, USA), the membranes were scanned using the Odyssey infrared imager (Li-Cor Biosciences) [16,17].

2.6. Statistical Analysis

Mann–Whitney tests and unpaired student *t*-tests using GraphPad Prism 5.0 were used to calculate the *p* values of the difference between viral titers and immune responses, respectively. Differences of *p* < 0.05 were considered significant.

3. Results

3.1. B.1.1.7 and B.1.351 Variants Replicate in the Lungs of C57BL/6 Mice

We inoculated six-week-old C57BL/6 mice with 10⁵ PFU of SARS-CoV-2 or PBS (mock) via the intranasal route. We used a representative virus from the original B.1 lineage, or

the emerging B.1.1.7 and B.1.351 lineages. We also infected a group of mice with a mouse-adapted SARS-CoV-2 variant (MA10) [11]. Mice were monitored daily for weight loss. Mice infected with B.1 virus exhibited no changes in body weight. However, B.1.1.7-, B.1.351- and MA10-infected mice had approximately 10% body-weight loss at days 2–4 after infection (Figure 1). To evaluate virus replication in the lungs, groups of 5–8 mice were euthanized at 3 days after infection, and the lungs were collected. Viral infectivity titers in the lungs were measured by plaque assay. The virus was not detected in the mock-infected lungs. High levels of infectious virus were detected in the lungs of all the MA10-infected mice (10^5 PFU/gram) (Figure 2A). By contrast, little, if any, infectious virus was detected in the lungs of the B.1-infected mice suggesting limited virus replication. High levels of infectious virus were detected in the lungs of both B.1.1.7- (10^4 PFU/gram) and B.1.351-infected mice (10^6 PFU/gram). The viral load was significantly lower for the B.1.1.7 compared with the B.1.351 virus. Virus titers in the lungs of the B.1.351-infected mice were higher than the MA10-infected mice, but the difference was not statistically significant. Intracellular SARS-CoV-2 RNA levels assessed by qRT-PCR followed a similar pattern. The viral RNA levels in the B.1.1.7-, B.1.351- and MA10-infected groups were significantly higher than those in the B.1-infected group (Figure 2B). These data indicate that MA10, B.1.1.7 and B.1.351 viruses replicated efficiently in the lungs of the infected animals, and the B.1.351 virus replicated to high titers in the lungs of mice compared with the other groups.

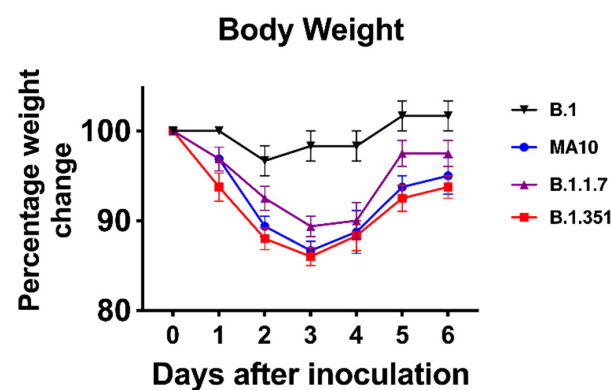


Figure 1. Analysis of body weight in C57BL/6 mice following SARS-CoV-2 infection. Six-week-old C57BL/6 mice were inoculated intranasally with 10^5 plaque-forming units (PFU) of SARS-CoV-2 variants ($n = 8–10$ mice per group). Percentage of initial weight for SARS-CoV-2-infected mice over 6 days. Values are the mean \pm SEM.

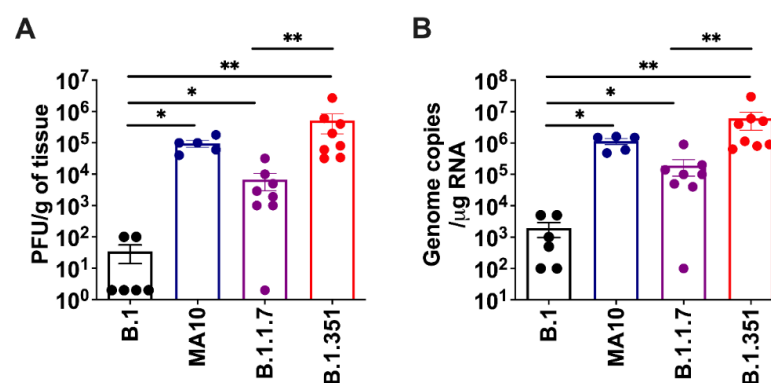


Figure 2. Replication of SARS-CoV-2 variants in the lungs. Six-week-old C57BL/6 mice were inoculated intranasally with PBS (mock) or 10^5 plaque-forming units (PFU) of SARS-CoV-2 variants. Groups of 5–8 mice were euthanized at 3 days after infection and lungs were collected. Virus titers were analyzed in the lungs by (A) plaque assay and (B) qRT-PCR. The data are expressed as PFU/g of tissue or genome copies/ μ g of RNA. Each data point represents an individual mouse. *, $p < 0.05$; **, $p < 0.001$.

3.2. B.1.1.7 and B.1.351 Variants Induce an Inflammatory Response in the Lungs

The excessive inflammatory host response to SARS-CoV-2 infection contributes to pulmonary pathology and the development of respiratory distress in some COVID-19 patients [20,21]. To compare the host responses in SARS-CoV-2-infected mice, we investigated changes in the mRNA levels of IL-6, TNF- α , IL-1 β and CCL2 in the lungs of mice infected with SARS-CoV-2. Gene expression changes in the lungs of infected mice, compared with the mock-infected controls, were analyzed by qRT-PCR. No significant increase in the mRNAs of the cytokines or chemokines tested was observed in the B.1-infected mice. MA10 infection resulted in a 20-fold increase in IL-6 and CCL2 mRNA expression (Figure 3). IL-1 β and TNF- α mRNA levels increased by 4–6-fold in the lungs of the MA10-infected mice. The B.1.351 infection resulted in a >25-fold increase in IL-6 and CCL2 mRNA expression. Similarly, TNF- α mRNA levels increased by 10-fold in the B.1.351-infected mice. There was also a 6-fold increase in IL-1 β mRNA in the B.1.351-infected mice. In the B.1.1.7-infected mice, the mRNA levels of the IL-6 and CCL2 were elevated by 10-fold. Although the expression of IL-1 β mRNA did not increase, a modest 3-fold increase in the TNF- α mRNA level was observed in the lungs of the B.1.1.7-infected mice. Inflammatory response observed in the B.1.351-infected group was significantly higher than in the B.1.1.7- and B.1-infected group. We also measured the protein levels of IL-6 in mock- and B.1.351-infected mice at day 3 after infection. Immunoblotting data showed an increase in the protein levels of IL-6 in the B.1.351-infected lungs, compared with the mock-infected controls (Figure 4). These results indicate that infection with B.1.351 and B.1.1.7 variants upregulates the expression of inflammatory genes in the lungs.

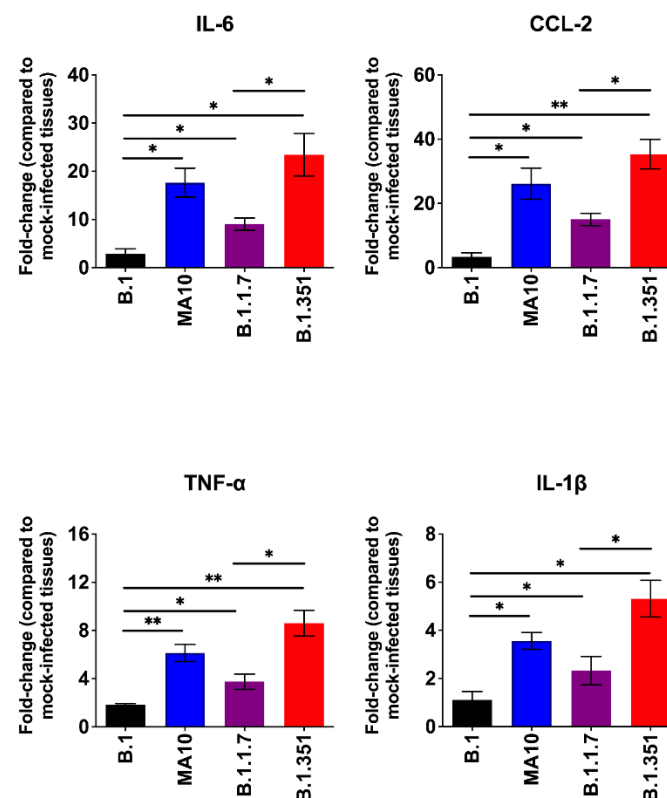


Figure 3. Analysis of inflammatory cytokine and chemokine levels in the lungs of SARS-CoV-2-infected mice. The mRNA levels of IL-6, CCL2, TNF- α and IL-1 β genes were determined by qRT-PCR. The fold change in the infected tissues compared to the corresponding mock-infected controls was calculated after normalizing individual samples to GAPDH levels. Values are the mean \pm SEM ($n = 5\text{--}8$ mice per group). *, $p < 0.05$; **, $p < 0.001$.

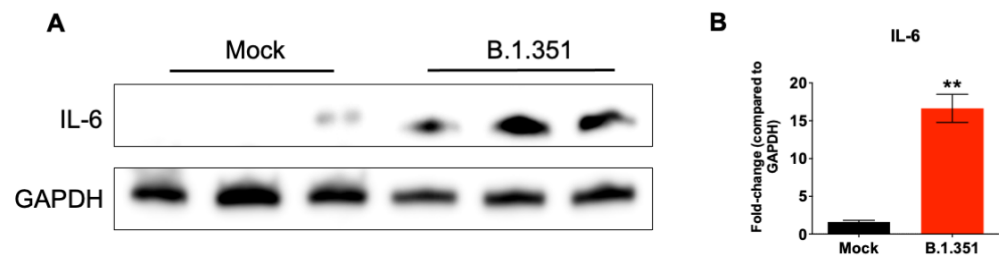


Figure 4. Analysis of protein levels of IL-6 in the lungs of B.1.351-infected mice. **(A)** Protein extracted from mock- and B.1.351-infected lung tissues (day 3 after infection) were immunoblotted with antibodies against IL-6 or GAPDH. Data are representative of five animals per group. **(B)** Quantitative analysis of Western blot results represented as fold-change compared to GAPDH. **, $p < 0.001$ as compared to mock controls ($n = 5$ mice per group).

We next analyzed the lung sections from mock- and B.1.351-infected mice for antigen distribution, infiltration of immune cells and other pathological changes. Immunostaining for the SARS-CoV-2 nucleocapsid revealed intense staining at day 3 after infection, consistent with the lung viral titer data (Figure 5). We also stained the lung sections with hematoxylin and eosin (HE) for histopathological evaluation. The histopathological features of the lungs infected with B.1.351 virus showed multifocal lesions with abundant leukocyte infiltration, hemorrhages and interstitial thickening. Representative images of lung sections from mock- or B.1.351-infected lungs on day 3 after infection are shown in Figure 6.

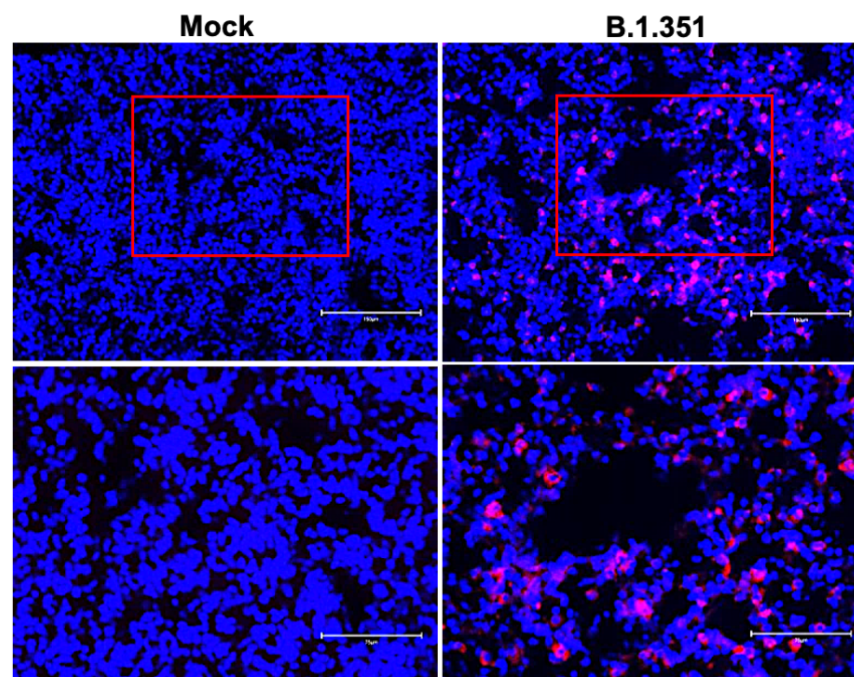


Figure 5. Detection of SARS-CoV-2-infected cells in the lungs of B.1.351-infected mice. Lung sections from mock- and B.1.351-infected mice (day 3 after infection) were stained for SARS-CoV-2 nucleocapsid protein. Representative immunostaining images showing the presence of SARS-CoV-2 nucleocapsid protein (red) in the B.1.351-infected mice. Nuclei are stained with DAPI (blue). The boxed areas in the top row of panels (20 \times) are enlarged in the bottom row of panels (40 \times). The photomicrographs shown are representative of the images obtained from five animals.

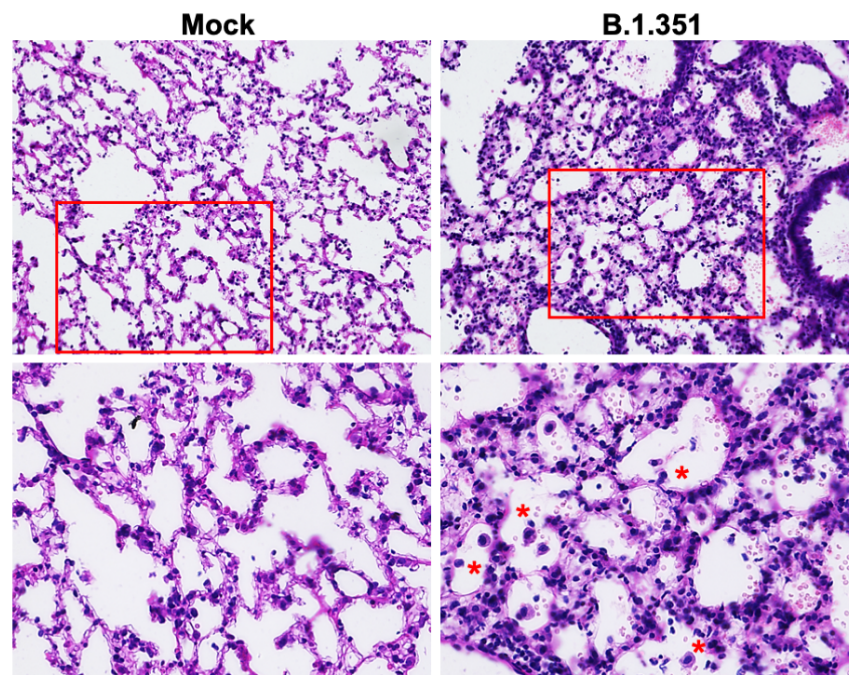


Figure 6. Histopathological analysis of B.1.351-infected lungs. Hematoxylin and eosin (HE) staining of lung sections from mock- and B.1.351-infected mice on day 3 after infection. Lung sections from infected mice showed multifocal lesions with abundant leukocyte infiltration (red asterisks), hemorrhages and interstitial thickening. The boxed areas in the top row of panels (20 \times) are enlarged in the bottom row of panels (40 \times). The photomicrographs shown are representative of the images obtained from five animals.

4. Discussion

This study demonstrates that wild-type laboratory mice are susceptible to infection with the emerging SARS-CoV-2 variants. While the B.1 virus was unable to infect C57BL/6 mice, the B.1.351 and B.1.1.7 viruses efficiently infected the C57BL/6 mice. Enhanced virus replication in the B.1.351- and B.1.1.7-infected mice was accompanied by elevated cytokine and chemokine levels and infiltration of leukocytes in the lungs.

Mice are a useful small animal model for the evaluation of vaccines, immunotherapies and antiviral drugs [8,12]. As the initial SARS-CoV-2 strains did not utilize murine ACE-2 as a receptor, wild-type mice are not susceptible to SARS-CoV-2 infection [8–10,12]. Transgenic mice that express human ACE-2 often develop severe and fatal disease upon intranasal inoculation of virus [16,22]. The initially available SARS-CoV-2 isolates require adaptation to use the mouse ACE-2 entry receptor, and to productively infect the cells of the murine respiratory tract. The mouse-adapted strain of SARS-CoV-2 (MA10) causes infection, inflammation and pneumonia in BALB/c mice after intranasal inoculation [11,13]. MA10 has several mutations, including the N501Y mutation in the RBD of the spike protein, compared with the Wuhan reference sequence, which also appears in the B.1.351 and B.1.1.7 variants [6,7,11,23]. These mutations in the RBD of the spike protein may have enhanced the binding affinity for the endogenous mouse ACE-2 receptor, thereby allowing the variants to replicate efficiently in mice. Indeed, studies have shown that SARS-CoV-2 variants containing N501Y and E484K mutations display a substantially enhanced infection of mouse cells. Experimental studies using S glycoprotein and pseudo type viruses have shown that SARS-CoV-2 variants are significantly more infective toward cells expressing murine ACE2 [23–26].

Although both B.1.351 and B.1.1.7 viruses were able to replicate in the mice lungs, B.1.351 virus inoculation yielded significantly higher viral load in the lungs than the B.1.1.7 virus. Both B.1.1.7 and B.1.351 variants shared the N501Y mutation that has been suggested to be associated with mouse adaptation [27]. Other differences between virus lineages

might also play a role in the resulting phenotype in mice. Apart from the N501Y mutation, several amino acid substitutions including, K417N, E484K, Q493H/K, and Q498H were also suggested to be critical for SARS-CoV-2 adaptation in murine species. It has been shown that the presence of E484K and K417N mutations in B.1.351 increase the infectivity of B.1.351, and E484K has also been identified as an immune escape mutation that emerges during exposure to antibodies [28]. This is congruous with our observation that B.1.351 virus replicated to a higher level than B.1.1.7 virus.

It has been suggested that a cytokine storm is involved in the pathogenesis of severe COVID-19 cases [20,21]. The levels of many cytokines and chemokines have been found to be increased after SARS-CoV-2 infection in humans. In the present study, we show that B.1.351 and B.1.1.7 infection induced significantly higher levels of cytokines and chemokine expression in the lungs. Inflammatory response observed in the B.1.351-infected group was higher compared with the other groups. In this study, we did not conduct a comprehensive transcriptome analysis of mice lungs that were infected with the B.1.351 and B.1.1.7 viruses. However, other recent studies have shown that intranasal infection of K18-hACE2 mice with B.1.1.7 and B.1.351 variants resulted in distinct arrays of cytokine response than those induced by early SARS-CoV-2 strains. Several myeloid cell chemoattractants showed enhanced pulmonary secretions in K18-hACE2 mice following exposures to B.1.1.7 or B.1.351 variant [29,30]. These findings are consistent with previous studies in humans, which established a consistent link between the mutations exhibited by the B.1.351 lineage and a greater potential for infectivity and immune escape [4,6,24]. More studies are needed to characterize the pathological consequences of infection with these variants in different mouse strains, and mice with co-morbid conditions. It is possible that more severe conditions could be observed in mice with co-morbid conditions such as old age, diabetes and hypertension. The ability of SARS-CoV-2 variants to replicate and induce inflammation in wild-type mice will facilitate studies to evaluate therapeutic interventions and pathogenesis studies using transgenic mouse strains. These data indicate the possibility of adaptation to new animal species by emerging SARS-CoV-2 variants.

Author Contributions: Conceptualization, M.K.; methodology, S.S. (Shannon Stone), H.A.R., J.P.N., P.K., K.A., T.T.A., S.S. (Shaligram Sharma), H.P. and M.K.; validation, H.A.R., S.S. (Shannon Stone), J.P.N., P.K. and M.K.; formal analysis, S.S. (Shannon Stone), H.A.R., J.P.N., P.K., K.A., S.S. (Shaligram Sharma), T.T.A., H.P. and M.K.; resources, M.K.; writing—original draft preparation, H.A.R. and M.K.; writing—review and editing, H.A.R., K.A. and M.K.; funding acquisition, M.K. All authors have read and agreed to the published version of the manuscript.

Funding: This work was supported by a grant (R21OD024896) from the Office of the Director, National Institutes of Health, and Institutional funds.

Institutional Review Board Statement: Not applicable.

Informed Consent Statement: Not applicable.

Data Availability Statement: Not applicable.

Acknowledgments: We thank members of the GSU High Containment Core and the Department for Animal Research for assistance with the experiments.

Conflicts of Interest: The authors declare no conflict of interest.

References

1. Rothan, H.A.; Byraredddy, S.N. The epidemiology and pathogenesis of coronavirus disease (COVID-19) outbreak. *J. Autoimmun.* **2020**, *109*, 102433. [[CrossRef](#)]
2. Kumar, M.; Iyer, S.S. ASSURED-SQVM diagnostics for COVID-19: Addressing the why, when, where, who, what and how of testing. *Expert Rev. Mol. Diagn.* **2021**, *21*, 349–362. [[CrossRef](#)]
3. Rothan, H.A.; Acharya, A.; Reid, S.P.; Kumar, M.; Byraredddy, S.N. Molecular Aspects of COVID-19 Differential Pathogenesis. *Pathogens* **2020**, *9*, 538. [[CrossRef](#)]
4. Walensky, R.P.; Walke, H.T.; Fauci, A.S. SARS-CoV-2 Variants of Concern in the United States—Challenges and Opportunities. *JAMA* **2021**, *325*, 1037–1038. [[CrossRef](#)]

5. SARS-CoV-2 Variant Classifications and Definitions. Available online: <https://www.cdc.gov/coronavirus/2019-ncov/variants/variant-info.html> (accessed on 10 December 2021).
6. Ramanathan, M.; Ferguson, I.D.; Miao, W.; Khavari, P.A. SARS-CoV-2 B.1.1.7 and B.1.351 spike variants bind human ACE2 with increased affinity. *Lancet Infect. Dis.* **2021**, *21*, 1070. [[CrossRef](#)]
7. Khan, A.; Zia, T.; Suleman, M.; Khan, T.; Ali, S.S.; Abbasi, A.A.; Mohammad, A.; Wei, D.Q. Higher infectivity of the SARS-CoV-2 new variants is associated with K417N/T, E484K, and N501Y mutants: An insight from structural data. *J. Cell Physiol.* **2021**, *236*, 7045–7057. [[CrossRef](#)]
8. Jia, W.; Wang, J.; Sun, B.; Zhou, J.; Shi, Y.; Zhou, Z. The Mechanisms and Animal Models of SARS-CoV-2 Infection. *Front. Cell Dev. Biol.* **2021**, *9*, 578825. [[CrossRef](#)] [[PubMed](#)]
9. Zhou, P.; Yang, X.L.; Wang, X.G.; Hu, B.; Zhang, L.; Zhang, W.; Si, H.R.; Zhu, Y.; Li, B.; Huang, C.L.; et al. A pneumonia outbreak associated with a new coronavirus of probable bat origin. *Nature* **2020**, *579*, 270–273. [[CrossRef](#)] [[PubMed](#)]
10. Dinno, K.H., 3rd; Leist, S.R.; Schafer, A.; Edwards, C.E.; Martinez, D.R.; Montgomery, S.A.; West, A.; Yount, B.L., Jr.; Hou, Y.J.; Adams, L.E.; et al. A mouse-adapted model of SARS-CoV-2 to test COVID-19 countermeasures. *Nature* **2020**, *586*, 560–566. [[CrossRef](#)] [[PubMed](#)]
11. Leist, S.R.; Dinno, K.H., 3rd; Schafer, A.; Tse, L.V.; Okuda, K.; Hou, Y.J.; West, A.; Edwards, C.E.; Sanders, W.; Fritch, E.J.; et al. A Mouse-Adapted SARS-CoV-2 Induces Acute Lung Injury and Mortality in Standard Laboratory Mice. *Cell* **2020**, *183*, 1070–1085. [[CrossRef](#)] [[PubMed](#)]
12. Munoz-Fontela, C.; Dowling, W.E.; Funnell, S.G.P.; Gsell, P.S.; Riveros-Balta, A.X.; Albrecht, R.A.; Andersen, H.; Baric, R.S.; Carroll, M.W.; Cavaleri, M.; et al. Animal models for COVID-19. *Nature* **2020**, *586*, 509–515. [[CrossRef](#)]
13. Gu, H.; Chen, Q.; Yang, G.; He, L.; Fan, H.; Deng, Y.Q.; Wang, Y.; Teng, Y.; Zhao, Z.; Cui, Y.; et al. Adaptation of SARS-CoV-2 in BALB/c mice for testing vaccine efficacy. *Science* **2020**, *369*, 1603–1607. [[CrossRef](#)]
14. Frampton, D.; Rampling, T.; Cross, A.; Bailey, H.; Heaney, J.; Byott, M.; Scott, R.; Sconza, R.; Price, J.; Margaritis, M.; et al. Genomic characteristics and clinical effect of the emergent SARS-CoV-2 B.1.1.7 lineage in London, UK: A whole-genome sequencing and hospital-based cohort study. *Lancet Infect. Dis.* **2021**, *21*, 1246–1256. [[CrossRef](#)]
15. Tegally, H.; Wilkinson, E.; Giovanetti, M.; Iranzadeh, A.; Fonseca, V.; Giandhari, J.; Doolabh, D.; Pillay, S.; San, E.J.; Msomi, N.; et al. Detection of a SARS-CoV-2 variant of concern in South Africa. *Nature* **2021**, *592*, 438–443. [[CrossRef](#)]
16. Kumari, P.; Rothan, H.A.; Natekar, J.P.; Stone, S.; Pathak, H.; Strate, P.G.; Arora, K.; Brinton, M.A.; Kumar, M. Neuroinvasion and Encephalitis Following Intranasal Inoculation of SARS-CoV-2 in K18-hACE2 Mice. *Viruses* **2021**, *13*, 132. [[CrossRef](#)]
17. Rothan, H.A.; Arora, K.; Natekar, J.P.; Strate, P.G.; Brinton, M.A.; Kumar, M. Z-DNA-Binding Protein 1 Is Critical for Controlling Virus Replication and Survival in West Nile Virus Encephalitis. *Front. Microbiol.* **2019**, *10*, 2089. [[CrossRef](#)] [[PubMed](#)]
18. Rothan, H.A.; Stone, S.; Natekar, J.; Kumari, P.; Arora, K.; Kumar, M. The FDA-approved gold drug auranofin inhibits novel coronavirus (SARS-CoV-2) replication and attenuates inflammation in human cells. *Virology* **2020**, *547*, 7–11. [[CrossRef](#)] [[PubMed](#)]
19. Natekar, J.P.; Rothan, H.A.; Arora, K.; Strate, P.G.; Kumar, M. Cellular microRNA-155 Regulates Virus-Induced Inflammatory Response and Protects against Lethal West Nile Virus Infection. *Viruses* **2019**, *12*, 9. [[CrossRef](#)] [[PubMed](#)]
20. Mangalmurti, N.; Hunter, C.A. Cytokine Storms: Understanding COVID-19. *Immunity* **2020**, *53*, 19–25. [[CrossRef](#)] [[PubMed](#)]
21. Blanco-Melo, D.; Nilsson-Payant, B.E.; Liu, W.C.; Uhl, S.; Hoagland, D.; Moller, R.; Jordan, T.X.; Oishi, K.; Panis, M.; Sachs, D.; et al. Imbalanced Host Response to SARS-CoV-2 Drives Development of COVID-19. *Cell* **2020**, *181*, 1036–1045. [[CrossRef](#)] [[PubMed](#)]
22. Zheng, J.; Wong, L.R.; Li, K.; Verma, A.K.; Ortiz, M.; Wohlford-Lenane, C.; Leidinger, M.R.; Knudson, C.M.; Meyerholz, D.K.; McCray, P.B., Jr.; et al. COVID-19 treatments and pathogenesis including anosmia in K18-hACE2 mice. *Nature* **2021**, *589*, 603–607. [[CrossRef](#)] [[PubMed](#)]
23. Yi, C.; Sun, X.; Ye, J.; Ding, L.; Liu, M.; Yang, Z.; Lu, X.; Zhang, Y.; Ma, L.; Gu, W.; et al. Key residues of the receptor binding motif in the spike protein of SARS-CoV-2 that interact with ACE2 and neutralizing antibodies. *Cell. Mol. Immunol.* **2020**, *17*, 621–630. [[CrossRef](#)] [[PubMed](#)]
24. Pearson, C.A.B.; Russell, T.W.; Davies, N.; Kucharski, A.J.; Edmunds, W.J.; Eggo, R.M.; CMMID COVID-19 Working Group. Estimates of Severity and Transmissibility of Novel SARS-CoV-2 Variant 501Y.V2 in South Africa. 2021. Available online: <https://cmmid.github.io/topics/covid19/sa-novel-variant.html> (accessed on 10 December 2021).
25. Niu, Z.; Zhang, Z.; Gao, X.; Du, P.; Lu, J.; Yan, B.; Wang, C.; Zheng, Y. N501Y mutation imparts cross-species transmission of SARS-CoV-2 to mice by enhancing receptor binding. *Signal Transduct. Target. Ther.* **2021**, *6*, 284. [[CrossRef](#)] [[PubMed](#)]
26. Yao, W.; Wang, Y.; Ma, D.; Tang, X.; Wang, H.; Li, C.; Lin, H.; Li, Y.; Zhong, G. Circulating SARS-CoV-2 variants B.1.1.7, 501Y.V2, and P.1 have gained ability to utilize rat and mouse Ace2 and altered in vitro sensitivity to neutralizing antibodies and ACE2-Ig. *BioRxiv* **2021**. [[CrossRef](#)]
27. Liu, Y.; Liu, J.; Plante, K.S.; Plante, J.A.; Xie, X.; Zhang, X.; Ku, Z.; An, Z.; Scharton, D.; Schindewolf, C.; et al. The N501Y spike substitution enhances SARS-CoV-2 infection and transmission. *Nature* **2021**. [[CrossRef](#)]
28. Weisblum, Y.; Schmidt, F.; Zhang, F.; DaSilva, J.; Poston, D.; Lorenzi, J.C.; Muecksch, F.; Rutkowska, M.; Hoffmann, H.H.; Michailidis, E.; et al. Escape from neutralizing antibodies by SARS-CoV-2 spike protein variants. *ELife* **2020**, *9*, e61312. [[CrossRef](#)]

29. Radvak, P.; Kwon, H.J.; Kosikova, M.; Ortega-Rodriguez, U.; Xiang, R.; Phue, J.N.; Shen, R.F.; Rozzelle, J.; Kapoor, N.; Rabara, T.; et al. SARS-CoV-2 B.1.1.7 (alpha) and B.1.351 (beta) variants induce pathogenic patterns in K18-hACE2 transgenic mice distinct from early strains. *Nature* **2021**, *12*, 6559. [[CrossRef](#)]
30. Winkler, E.S.; Bailey, A.L.; Kafai, N.M.; Nair, S.; McCune, B.T.; Yu, J.; Fox, J.M.; Chen, R.E.; Earnest, J.T.; Keeler, S.P.; et al. SARS-CoV-2 infection of human ACE2-transgenic mice causes severe lung inflammation and impaired function. *Nat. Immunol.* **2020**, *21*, 1327–1335. [[CrossRef](#)]